Intermittency in a Piecewise-Linear Circuit

Leon O. Chua, *Fellow*, *IEEE*, and Gui-nian Lin

***Abstract*—In this paper we present the first example of the intermittency phenomenon observed from the canonical realization of the Chua's circuit family. The intermittency has been confirmed both by experiments on the laboratory circuit, and by computer simulation of the circuit model. An analysis of the geometrical structure of the vector field is also presented and the mechanism of the intermittency is identified.**

I. Introduction

Over the past decade, piecewise-linear circuits have emerged as a simple yet powerful experimental and analytical tool in studying bifurcation and chaos in nonlinear dynamics. Among the many piecewise-linear circuits that have been studied, there is one particularly important group whose state equations are linearly conjugate to members of the *Chua's circuit family* [1] that has been investigated in depth. Each member of this family consists of linear resistors, three linear dynamic elements (capacitors and/or inductors), and a nonlinear resistor characterized by a three-segment symmetric piecewise linear v-i characteristics. Double scroll, torus, and other interesting attractors and dynamic phenomena have been observed from different members of this family [2]–[7].

There are three well-known routes to chaos. The double scroll attractor is a typical example of a pitchfork bifurcation from a periodic orbit to chaos via a period-doubling route. The second (Ruelle–Takens–Newhouse) route, which leads to chaos via three successive stages of Hopf bifurcations, has also been observed [4]. The third route to chaos is the Manneville–Pomeau intermittency route. The key feature of this route is as follows. Over a certain range of a parameter the dynamic system has a periodic orbit. As the parameter is tuned beyond a critical value, some irregular short bursts appear among the long regular phases. As the value of the parameter changes further, the bursts appear more frequently and the average time between two consecutive bursts shortens. Eventually the system moves into a chaotic regime. The phenomenon associated with this route is a saddle-node bifurcation, which is different qualitatively from those in the other two routes. In this paper we will report the first example of intermittency recently observed from a canonical circuit realization of the Chua's circuit family [8].

Manuscript received March 8, 1990; revised December 9, 1990. This work was supported in part by the Office of Naval Research under Contract N00014-89-J1402, and by the National Science Foundation under Grant MIP-8614000. This paper was recommended by Associate Editor H. D. Chiang.

L. O. Chua is with the Department of Electrical Engineering and Computer Sciences, University of California, Berkeley, CA 94720.

G.-N. Lin is with the Department of Electrical Engineering and Computer Sciences, University of California, Berkeley, CA 94720, on leave from the Shanghai Railroad Institute, China.

IEEE Log Number 9143179.

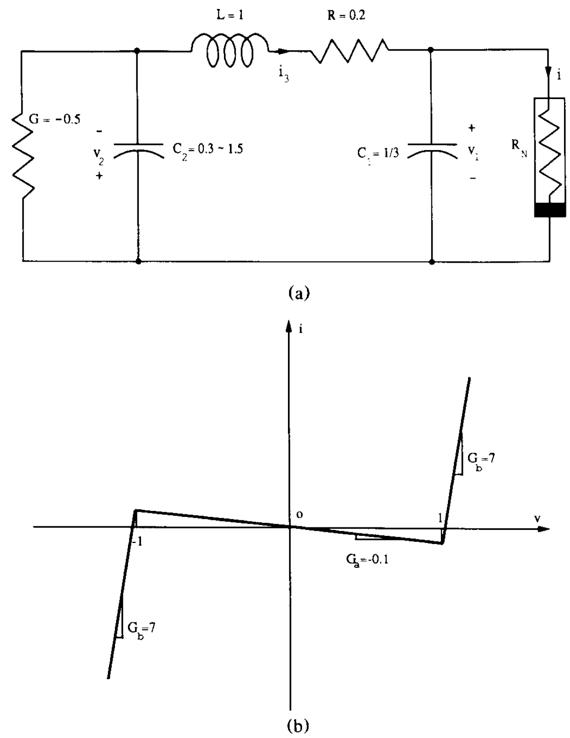

Fig. 1. (a) The canonical realization of the Chua's circuit family. (b) The v-i characteristic of the nonlinear resistor G_N.

In Section II, we present the results from experimental observations of this intermittency phenomenon in our laboratory circuit. In Section III, we present the results from computer simulation of the circuit model. Finally in Section IV, we present an analysis of the geometrical structure of the associated vector field and identify the mechanism which give rise to intermittency in this system.

II. Experimental Observation

The six-element circuit shown in Fig. 1(a) is a canonical realization of the Chua's circuit family. Fig. 1(b) shows the v-i characteristic of the piecewise-linear resistor R_N in Fig. 1(a). This circuit is called a *canonical realization*

0098-4094/91/0500-0510$01.00 ©1991 IEEE

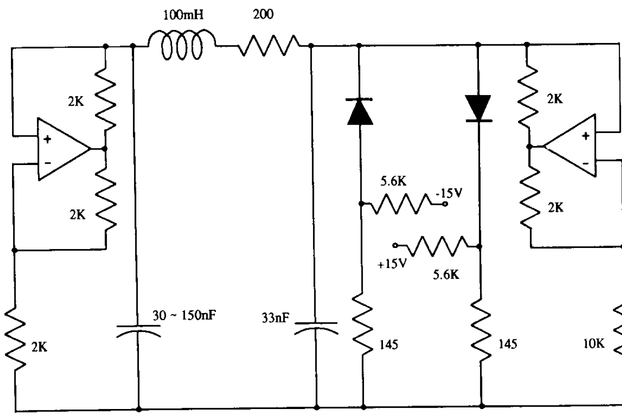

Fig. 2. Laboratory realization of the circuit in Fig. 1(a).

because it can produce *all* vector fields that could be produced by the entire Chua's circuit family and it contains the *minimum* number of elements needed for such a purpose.

The parameters of the elements used in this paper are:

$$C_1 = \frac{1}{3}, \qquad G = -0.5, \qquad G_a = -0.1,$$
$$G_b = 7, \qquad L = 1, \qquad R = 0.2. \qquad (1)$$

C_2 is an adjustable parameter. Its value varies approximately between 0.3 to 1.5.

Fig. 2 shows the laboratory realization of the circuit in Fig. 1. In order to normalize the physical values of the circuit elements to a reasonable range, we adopt the following normalization scale:

$$v_0 = 1\text{ V}, \qquad i_0 = 1\text{ mA}, \qquad C_0 = 100\text{ nF},$$
$$L_0 = 100\text{ mH}, \qquad R_0 = 1\text{ k}\Omega. \qquad (2)$$

The left part of Fig. 2 is a realization of the negative admittance $G = -1/2$. The right part of the figure is a realization of the piecewise-linear resistor R_N. The op-amp circuit is used to realize the negative slope of R_N, i.e., $G_a = -0.1$. Two diodes with series resistors realize the positive slope $G_b = 7$. The ± 15-V voltages connected to the diodes ensure that the break points occur at $v_1 = \pm 1$. The remaining elements in Fig. 2 are obtained by multiplying the (dimensionless) element value in Fig. 1(a) by the corresponding normalization constant in (2).

Fig. 3 shows a series of Lissajou's figures obtained from the circuit. When we start from $C_2 = 40$ nF, the $v_1 - v_2$ Lissajou's figure is a symmetric limit cycle (Fig. 3(a)). As C_2 increases and reaches a critical value, this symmetric limit cycle splits into two asymmetric limit cycles, which are symmetric to each other. Fig. 3(b) shows one of them. As C_2 increases further, *intermittency* eventually occurs. In Fig. 3(c), we can see a bright area of dense trajectories whose boundary resembles the limit cycle in Fig. 3(b), along with some sparse trajectory loci connected to this bright strip. The brightness of the "strip" indicates that the trajectory spent much more time in this area than in the other.

We have also photographed the time waveforms. The periodic waveform shown in Fig. 4(a) corresponds to the limit cycle in Fig. 3(b). Fig. 4(b) shows a part of the waveform associated with the trajectory in Fig. 3(c). It consists of a long regular phase and is followed by a short burst. This is the typical feature of intermittency. As C_2 increases further, the regular phases get shorter and the bursts appear more frequently, as indicated by Fig. 4(c). Finally the waveform looks completely chaotic, as shown in Fig. 4(d). The corresponding chaotic Lissajou's figure is shown in Fig. 3(d). Between Fig. 3(c) and (d), we can also observe some periodic windows. If C_2 is increased beyond the range that gives rise the chaotic attractor in Fig. 3(d), half of the attractor suddenly disappears as shown in Fig. 3(e). As C_2 increases further, this chaotic attractor will gradually shrink and eventually become a periodic limit cycle. Fig. 3(f) shows a period-4 limit cycle. Immediately after that we will get a period-2 limit cycle, as shown in Fig. 3(g). As C_2 increases further, this limit cycle shrinks gradually and eventually becomes an elliptical orbit, as shown in Fig. 3(h), whose waveform is a nearly sinusoidal oscillation. At last, if C_2 is large enough, this sinusoidal oscillation will shrink to an equilibrium point.

Fig. 5 gives the complete bifurcation scenario for different values of C_2. There are three major bifurcations, each of a different character. As C_2 increases (from the left) and reaches the first critical value C_a, a pitchfork bifurcation occurs which splits the symmetric limit cycle into two asymmetric limit cycles. As C_2 increases further and reaches the next critical value C_b, a saddle-node bifurcation takes place. The asymmetric limit cycle loses its stability, as manifested by the appearance of some irregular short bursts. On the other hand, if we start with a large enough value for C_2 and decrease its value, we would encounter yet another critical value C_c, where a Hopf bifurcation at the equilibrium point will give rise to a nearly sinusoidal oscillation. As C_2 decreases further, we encounter a series of pitchfork bifurcations (period-doubling route) that eventually leads to chaos. Thus, starting from C_b or C_c, the system can enter the chaotic regime via different routes. In addition, in the chaotic region we have also observed some periodic windows. However, since the main topic of this paper is intermittency, we will focus our attention on the bifurcation phenomenon around C_b.

III. Computer Simulation

The state equations of the circuit in Fig. 1(a) are given by

$$\left.\begin{aligned} \frac{dv_1}{dt} &= \frac{1}{C_1}[-f(v_1)+i_3] \\ \frac{dv_2}{dt} &= \frac{1}{C_2}(-Gv_2+i_3) \\ \frac{di_3}{dt} &= \frac{-1}{L}(v_1+v_2+Ri_3) \end{aligned}\right\} \quad (3)$$

where

$$f(v) = G_b v + \frac{1}{2}(G_a - G_b)(|v+1| - |v-1|) \quad (4)$$

is the v-i characteristic of the nonlinear resistor shown in Fig. 1(b).

Before we undertake a detailed analysis of (3), which comes from the *ideal* circuit in Fig. 1(a), let us first verify that the experimental results *measured* from the laboratory circuit in Fig. 2 can be reproduced by the dynamical equation (3), via computer simulation. Using the software INSITE [9], [10], we plotted some trajectories for (3) using the parameter values listed in (1). Fig. 6(a)–(h) are the counterparts of those in Fig. 3(a)–(h). Observe that each pair of these pictures are qualitatively the same. Moreover, the corresponding values of C_2 differ only slightly, due to the tolerance of the circuit elements in the laboratory realization.

Also we have investigated the following numerical aspects of this circuit: characteristic multipliers, average length of the regular phases, amplitude plot, and Lyapunov exponents. Results from all these aspects confirm the existence of intermittency.

3.1. Characteristic Multipliers

For $C_2 < C_b$, the circuit exhibits periodic solutions as shown in Fig. 6(a)–(b). Let us consider the Poincare map of the orbit. Pick an arbitrary plane (e.g., $i_3 = 0$). For a periodic orbit the fixed point of the Poincare map is stable and the two eigenvalues of the corresponding Poincare map are located inside the unit-circle. The eigenvalues are also called *characteristic multipliers*, or Floquet multipliers.

For $C_2 > C_b$, the intermittency starts and the periodic limit cycle is no longer stable. This implies that at least one of the characteristic multipliers must cross the unit

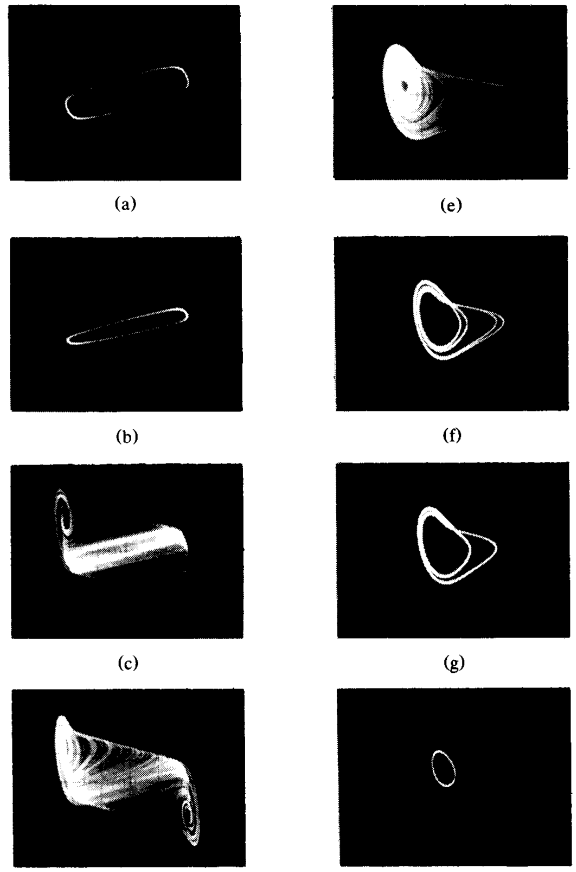

Fig. 3. Lissajou's figures of $(v_1(t), v_2(t))$ of the circuit in Fig. 2. Horizontal scale: 0.5 V/div in (a)–(d) and 0.2 V/div in (e)–(h); vertical scale: 1 V/div in (a)–(d) and 0.5 V/div in (e)–(h). Position in the center of the screen: (0,0) in (a)–(d) and $(-1, 1)$ in (e)–(h). (a) $C_2 = 40$ nF: a symmetric limit cycle. (b) $C_2 = 53$ nF: an asymmetric limit cycle. (c) $C_2 = 53.8$ nF: intermittency starts. (d) $C_2 = 70$ nF: a chaotic attractor. (e) $C_2 = 80$ nF: a chaotic attractor, which looks like the upper-left half of the attractor in (d). (f) $C_2 = 102$ nF: a period-4 limit cycle. (g) $C_2 = 106$ nF: a period-2 limit cycle. (h) $C_2 = 125$ nF: a nearly sinusoidal oscillation.

circle when C_2 reaches C_b. Using the numerical algorithm described below, we calculated the characteristic multipliers near C_b. Our algorithm proceeds as follows: First, use the Newton–Raphson algorithm to find a periodic trajectory. If the algorithm converges, there is a periodic orbit. Then, construct two orthogonal vectors, $\vec{A}$: $(v_1, v_2) = (1,0)$ and $\vec{B}$: $(v_1, v_2) = (0,1)$. Using the variational equation of the original nonlinear system, we calculate the maps of the vectors $\vec{A}$ and $\vec{B}$. Suppose their maps are $\vec{A}_1 = (a_1, a_2)$ and $\vec{B}_1 = (b_1, b_2)$, then the characteristic multipliers m_1 and m_2 are found by calculating the two roots of the following quadratic equation:

$$m^2 - (a_1 + b_2)m + (a_1 b_2 - a_2 b_1) = 0. \quad (5)$$

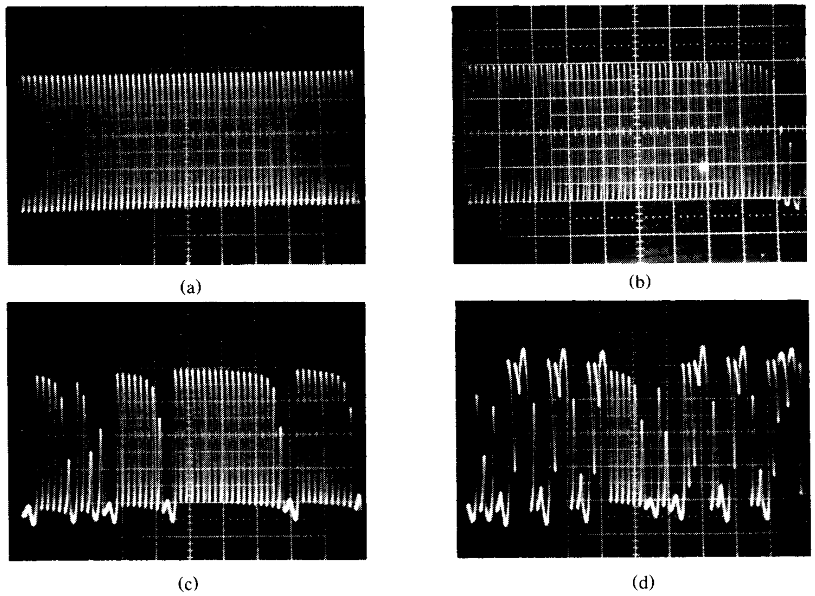

Fig. 4. Waveforms of $v_1(t)$ of the circuit in Fig. 2. Horizontal scale: 2 ms/div; vertical scale: 0.5 V/div. (a) $C_2 = 53$ nF: a periodic waveform. (b) $C_2 = 53.8$ nF: long regular phase with short burst. (c) $C_2 = 56$ nF: regular phases get shorter and bursts appear more frequently. (d) $C_2 = 70$ nF: a completely chaotic waveform.

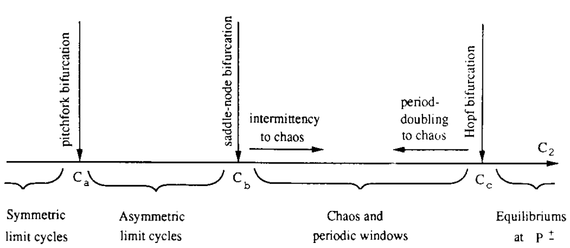

Fig. 5. Bifurcation scenario when C_2 in Fig. 2 varies.

For the range of C_2 used in our numerical algorithm, multipliers are found to be real numbers inside the unit circle, and only the one tending towards 1 is graphed in Fig. 7. Observe that when C_2 approaches the value C_b, somewhere between 0.558 and 0.559, this characteristic multiplier approaches +1.

Hence, among the three types of intermittent phenomena (depending on where an eigenvalue crosses the unit circle [11]), our numerical results show that the phenomenon we observed is a *type-1 intermittency*.

3.2. Average Length

For $C_2 > C_b$, Figs. 3(c) and 6(c) show that the trajectories spent a long time oscillating in the regular phases. In this regime, the trajectories are nearly periodic. The shape of the Lissajou's figure during each "period" is very similar to the limit cycle in Figs. 3(b) and 6(b). However, they are not really periodic. Instead, each consecutive "period" is seen to shift by a very small amount. Moreover, when the total displacement has accumulated to a certain threshold value, a sudden burst is seen to take place. Immediately after the burst, the trajectory appears to be chaotic until it is reinjected into the regular phase, sooner or later. The time between two bursts is not fixed and seems random. We can estimate only its average value. For different values of C_2, we have estimated the average length of the regular phases between 100 bursts. This length is estimated by counting the number of "periods" between every two consecutive bursts and the results are shown in Fig. 8. It is known that the scaling law for a type-1 intermittency is given by [11]

$$l \propto (C_2 - C_b)^{-1/2}.$$

Observe that the empirical curve in Fig. 8 is quite close to this law.

3.3. Amplitude Plot

Recall that the trajectory in the regular phases looks "periodic" but with each period changing slightly. For simplicity let us refer to the maximum value of the v_1 coordinate in each "period" as the "amplitude." Considering two consecutive amplitudes as a one-dimensional map (i.e., taking the new amplitude as a function of the last amplitude), we can draw the associated amplitude plot, or the Lorenz plot. Fig. 9 shows this plot, where we have also plotted the unit-slope diagonal line for comparison purposes. Since the one-dimensional map is very close to this diagonal line, they are almost indistinguishable in some areas. Observe that the one-dimensional map is always located beneath the diagonal, and is unstable

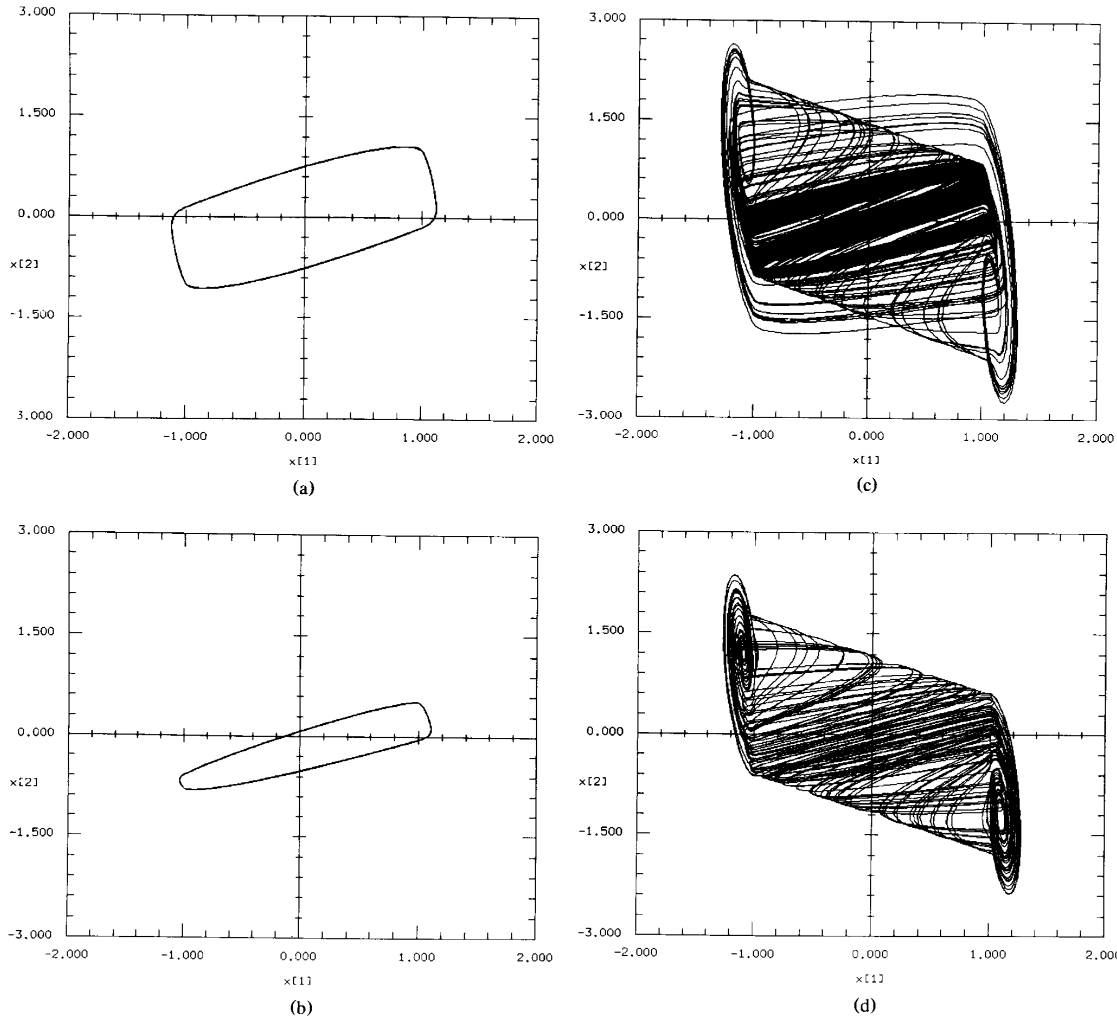

Fig. 6. Trajectories of (v_1, v_2) of the circuit in Fig. 1 from computer simulation. (a) $C_2 = 0.40$: a symmetric limit cycle. (b) $C_2 = 0.558$: an asymmetric limit cycle. (c) $C_2 = 0.56$: intermittency starts. (d) $C_2 = 0.72$: a chaotic attractor. (e) $C_2 = 0.80$: a chaotic attractor, which looks like the upper-left half of the attractor in (d). (f) $C_2 = 1.325$: a period-4 limit cycle. (g) $C_2 = 1.36$: a period-2 limit cycle. (h) $C_2 = 1.449$: a nearly sinusoidal oscillation.

(slope > 1) near the origin. There is a very narrow gap between the amplitude plot and the diagonal. This narrow gap forces the trajectory to oscillate a long time before it diverges towards the origin. As the amplitude decreases towards 1, the gap becomes wider. This means that the amplitude will change drastically once it enters this area. Then the trajectory looks chaotic and traverses wildly. Sooner or later, however, it will reinject into the narrow gap and the same phenomenon will repeat itself. However, since the reinjection process is "random" and since there is no fixed entry point for the reinjection, the "length" of the regular phases appears somewhat "random." This means that for a given set of parameters, the long-term waveform is never repeated, while the short-term waveforms could vary wildly. Some regular phases are shorter, while others are longer. Also, short-term waveforms sampled from circuits with different parameters could look alike. However, for different values of parameters, even though similar short-term waveforms could appear, the probabilities of their appearance are different.

3.4. *Lyapunov Exponents*

We have also calculated the Lyapunov exponents for various values of C_2 around C_b. Our algorithm for calculating Lyapunov exponents is based on its definition and the Gram–Schmidt orthonormalization technique [10]. However, one point should be mentioned: Since the average length of the regular phases can be extremely long at

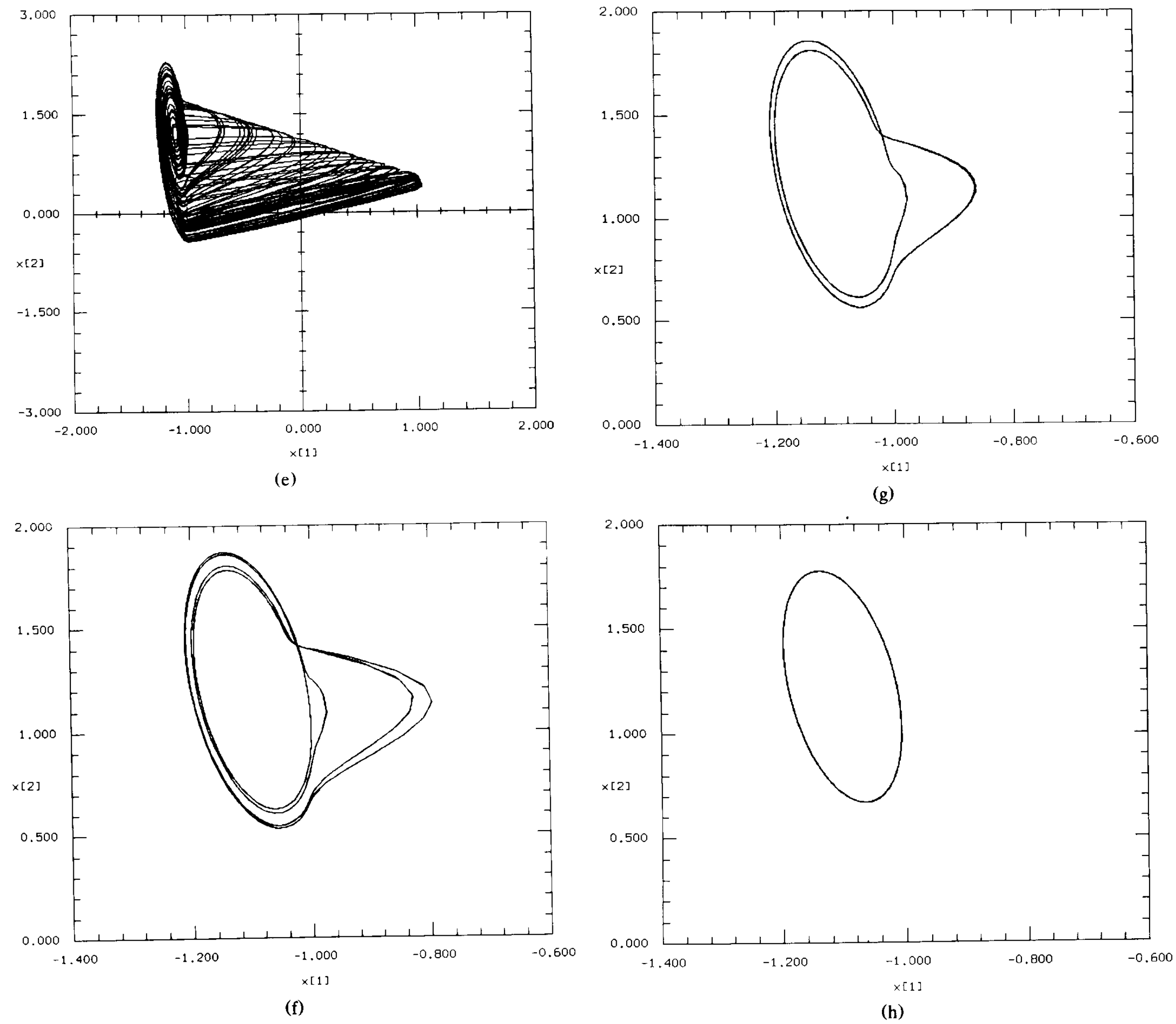

Fig. 6. Continued

values of C_2 just beyond C_b, in order to estimate the Lyapunov exponents accurately, we must calculate them over long lapses of time. Otherwise, the intermittency regime cannot be distinguished from the periodic regime and the numerical results would be misleading. Fig. 10 shows the first and second Lyapunov exponents we have estimated. For $C_2 < C_b$, the first Lyapunov exponent λ_1 is almost zero, as it should be since the trajectory is periodic. The second Lyapunov exponent λ_2 is negative and increases towards zero. This coincides with the increase of characteristic multiplier m_1 towards $+1$. It is known that λ_2 and m_1 for a T-periodic trajectory must follow the relationship [10]:

$$\lambda_2 = \frac{1}{T} \ln m_1. \tag{6}$$

In Fig. 10 we have also plotted (denoted by small squares) the values of λ_2 as calculated from (6) using the data for m_1 in Fig. 7. The results are quite close, which also justifies our algorithm.

IV. Analysis

In this section we will present an analysis of the geometrical structure of the vector field defined by (3) and will identify the mechanism of intermittency in our circuit.

For simplicity let us denote (v_1, v_2, i_3) by $\boldsymbol{x} = (x, y, z)$. The $\boldsymbol{R}^3$ space of (x, y, z) is divided by two boundary planes U_1: $x = 1$ and U_{-1}: $x = -1$. The subspace between U_1 and U_{-1} is denoted by D_0 and the subspaces above U_1 and below U_{-1} are denoted by D_{+1} and D_{-1}, respectively. The vector field in the $\boldsymbol{R}^3$ space is continuous, symmetric with respect to the origin, and piecewise linear. The origin is obviously an equilibrium point. The sub-

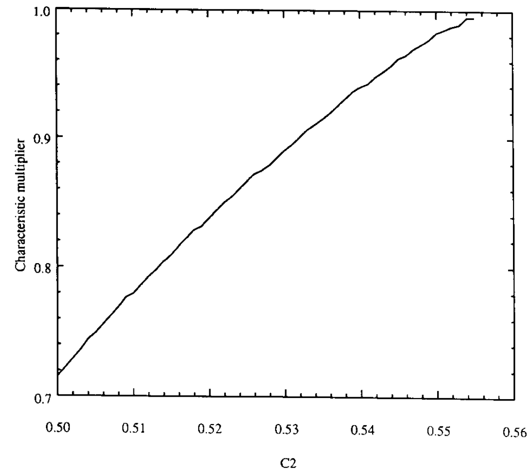

Fig. 7. The plot of the characteristic multiplier m_1 versus the parameter C_2.

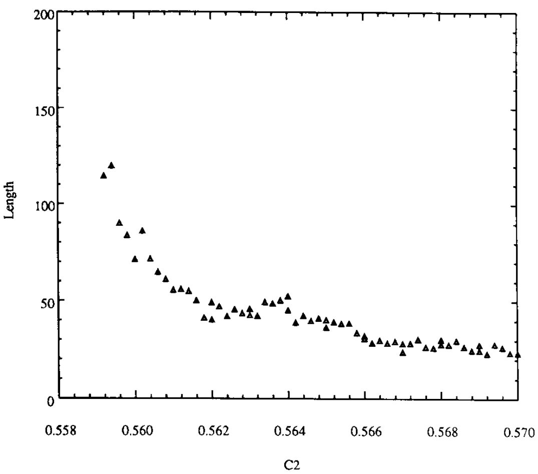

Fig. 8. The plot of the average length versus the parameter C_2.

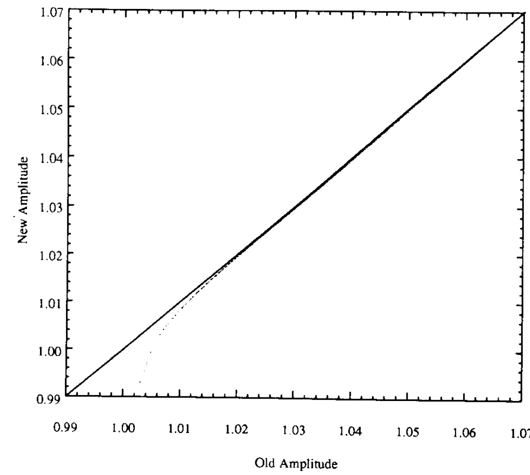

Fig. 9. The amplitude plot. $C_2 = 0.56$.

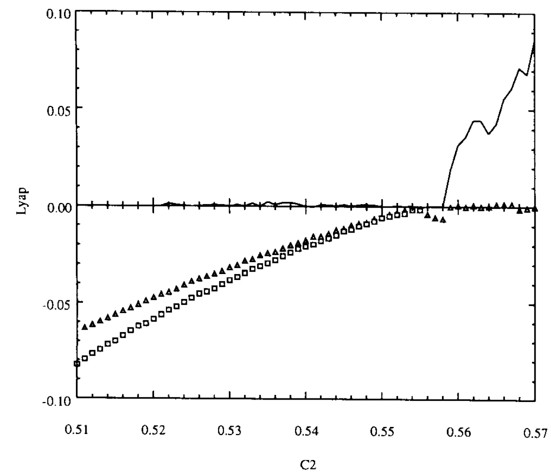

Fig. 10. The Lyapunov exponents versus C_2 plot. The solid curve is the first Lyapunov exponent λ_1. The upper curve (denoted by small triangles) below the axis is the second Lyapunov exponent λ_2 obtained from direct calculations, while the lower curve (denoted by small squares) is λ_2 calculated from (6).

spaces $D_{\pm 1}$ may or may not have equilibrium points, depending on whether the inequality

$$(G + G_a(1+GR))(G + G_b(1+GR) < 0 \tag{7}$$

is satisfied or not [8]. For the parameter values given in (1), (7) is satisfied. Therefore, D_{+1} and D_{-1} have equilibrium points P^+ and P^-, respectively. From (3), the coordinates of $P^{\pm}$: $(\pm x_p, \pm y_p, \pm z_p)$ is given by

$$(x_p, y_p, z_p) = \left(\frac{(G_b - G_a)(1+GR)}{G_b + G(1+RG_b)}, \frac{-(G_b - G_a)}{G_b + G(1+RG_b)}, \frac{-G(G_b - G_a)}{G_b + G(1+RG_b)} \right). \tag{8}$$

Since the dynamic behavior of any member of the Chua's circuit family is determined completely by the six eigenvalues [3], let us consider the eigenvalues of our circuit. In the D_0 region the state equation (3) becomes linear:

$$\begin{bmatrix} \dfrac{dv_1}{dt} \\ \dfrac{dv_2}{dt} \\ \dfrac{di_3}{dt} \end{bmatrix} = \begin{bmatrix} \dfrac{-G_a}{C_1} & 0 & \dfrac{1}{C_1} \\ 0 & \dfrac{-G}{C_2} & \dfrac{1}{C_2} \\ \dfrac{-1}{L} & \dfrac{-1}{L} & \dfrac{-R}{L} \end{bmatrix} \begin{bmatrix} v_1 \\ v_2 \\ i_3 \end{bmatrix} = \boldsymbol{M}_0 \begin{bmatrix} v_1 \\ v_2 \\ i_3 \end{bmatrix} \tag{9}$$

where $\boldsymbol{M}_0$ is a constant matrix. The characteristic equation of M_0 is:

$$|s1 - M_0| = s^3 + s^2\left(\frac{G_a}{C_1} + \frac{G}{C_2} + \frac{R}{L}\right) + s\left(\frac{GG_a}{C_1C_2} + \frac{G_aR}{LC_1} + \frac{GR}{LC_2} + \frac{1}{LC_1} + \frac{1}{LC_2}\right) + \frac{G + G_a + GG_aR}{LC_1C_2} = 0. \quad (10)$$

Substituting all parameter values into (10) and solving the cubic equation, we obtain three eigenvalues in D_0. The three eigenvalues in $D_{\pm 1}$ can be obtained the same way with G_a replaced by G_b. For the parameters given in (1) and $C_2 = 0.56$, the eigenvalues in D_0 and $D_{\pm 1}$ consists of a real and a pair of complex-conjugate values, namely:

$$\gamma_0 = 0.686417, \qquad \sigma_0 \pm j\omega_0 = 0.153220 \pm j2.14037$$
$$\gamma_1 = -20.8554, \qquad \sigma_1 \pm j\omega_1 = 0.274096 \pm j1.18942. \quad (11)$$

The eigenspace corresponding to a real eigenvalue is a line and will be denoted by E^r. The eigenspace corresponding to a pair of complex-conjugate eigenvalues is a plane spanned by the real and imaginary parts of the complex-conjugate eigenvectors and will be denoted by E^c. After some algebraic manipulations, we obtain the equations of the eigenspaces in the following explicit forms:

$$E^r(0): \quad \frac{x}{C_2\gamma_0 + G} = \frac{y}{C_1\gamma_0 + G_a} = \frac{z}{(C_1\gamma_0 + G_a)(C_2\gamma_0 + G)}$$

$$E^c(0): \quad C_1\left(\omega_0^2 + \left(\sigma_0 + \frac{G_a}{C_1}\right)^2\right)x - C_2\left(\omega_0^2 + \left(\sigma_0 + \frac{G}{C_2}\right)^2\right)y + \left(\frac{G}{C_2} - \frac{G_a}{C_1}\right)z = 0$$

$$E^r(P^\pm): \quad \frac{x \mp x_P}{C_2\gamma_1 + G} = \frac{y \mp y_P}{C_1\gamma_1 + G_a} = \frac{z \mp z_P}{(C_1\gamma_1 + G_a)(C_2\gamma_1 + G)}$$

$$E^c(P^\pm): \quad C_1\left(\omega_1^2 + \left(\sigma_1 + \frac{G_b}{C_1}\right)^2\right)(x \mp x_P) - C_2\left(\omega_1^2 + \left(\sigma_1 + \frac{G}{C_2}\right)^2\right)(y \mp y_P) + \left(\frac{G}{C_2} - \frac{G_b}{C_1}\right)(z \mp z_P) = 0. \quad (12)$$

Fig. 11 shows the geometric structure of the eigenspaces corresponding to the eigenvalues calculated in (11). In the figure we have also plotted the lines L_0, L_1, L_2 and the fundamental points A, B, C, D, E, defined as follows [3]:

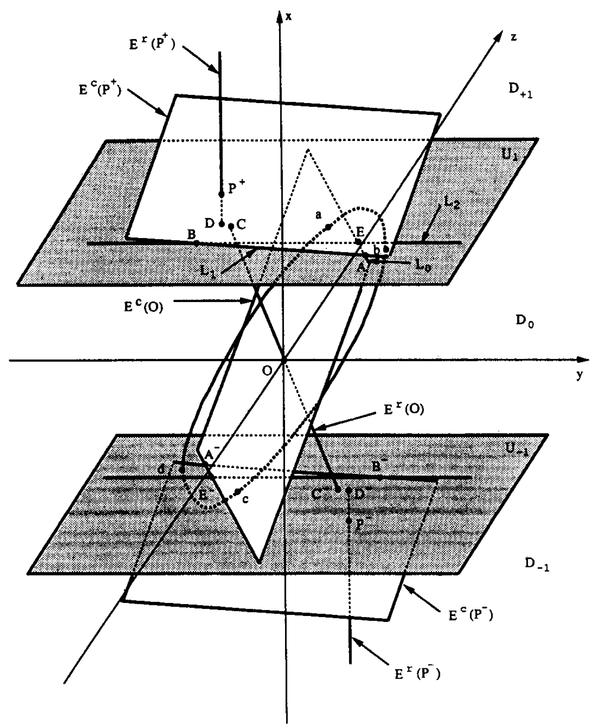

Fig. 11. The geometric structure of the intermittency system.

$$L_0 = E^c(O) \cap U_1$$
$$L_1 = E^c(P^+) \cap U_1$$
$$L_2 = \{x \in U_1 : \dot{x} = 0\}$$
$$A = L_0 \cap L_1$$
$$B = L_1 \cap L_2$$
$$C = E^r(O) \cap U_1$$
$$D = E^r(P^+) \cap U_1$$
$$E = L_0 \cap L_2. \quad (13)$$

The equation of the line L_2 is simply $x = 1$ and $z = G_a$. The positions of the other lines and the fundamental points can also be determined from (8), (12), and (13).

Let us analyze a typical trajectory in this system. The vector field on the U_1 plane is divided by the line L_2 as follows. The vector field of every point on the U_1 plane but above the line L_2 is directed upwards while the vector field of every point on the U_1 plane but below the line L_2 is directed downwards. Because $\gamma_1 < 0$, any trajectory that penetrates U_1 from below will be sucked towards the $E^c(P^+)$ plane. However, since $E^c(P^+)$ is an eigenspace, the trajectory can never penetrate it. Theoretically, a trajectory needs an infinite amount of time to reach $E^c(P^+)$ and therefore never actually does. At the same time, since $\sigma_1 > 0$, the trajectory will rotate outwards around the axis of $E^r(P^+)$. Due to the combination of these two motions, the trajectory will eventually intersect the U_1 plane in the wedge area subtended by $\angle ABE$. After the trajectory penetrates the U_1 plane from above and re-enters the D_0 region, it will be subject to two new motions due to $\gamma_0 > 0$ and $\sigma_0 > 0$: diverging from the $E^c(O)$ plane and rotating outwards around the axis of $E^r(O)$. For simplicity, let us denote the area $\angle ABE \setminus \Delta ABE$ by $\overline{\Delta ABE}$ and denote the area of $\angle A^-B^-E^- \setminus \Delta A^-B^-E^-$ by $\overline{\Delta A^-B^-E^-}$. Any trajectory starting from a point $x \in \overline{\Delta ABE}$ will move downwards until it hits the U_{-1} plane, while any trajectory starting from a point $x \in \Delta ABE$ will either hit the U_{-1} plane, or come back to hit the U_1 plane. As for the trajectories starting from $x \in \overline{AE}$, they will move downwards but constrained all the time on the $E^c(O)$ plane before hitting the line $\overline{A^-E^-}$ at some finite time.

Compared to the double scroll dynamics, we observe the following significant differences:

1) In the double scroll dynamics, we have $\gamma_0 > 0$ and $\sigma_0 < 0$. But in our present intermittency dynamics, we have $\gamma_0 > 0$ and $\sigma_0 > 0$.
2) In the double scroll dynamics, the trajectory starting from any point $x \in \overline{AE}$ needs an infinite time to return to either U_1 or U_{-1} plane. But in our present intermittency dynamics, it always hits the U_{-1} plane in some finite time.
3) In the double scroll dynamics, two trajectories starting from points immediately adjacent to the right and left side of the line $\overline{AE}$ will hit two different planes, U_1 and U_{-1}. But in our present intermittency dynamics, they will both hit the U_{-1} plane.

Therefore, we can expect the dynamic behavior of our present system to be quite different from that of the double scroll system. When we start our computer simulation from a small value of C_2, the trajectory is a symmetric limit cycle (see Fig. 6(a)). In this situation the trajectory enters the D_0 region through $\overline{\Delta ABE}$ and $\overline{\Delta A^-B^-E^-}$, as depicted in Fig. 11. In Fig. 11 we denote the four intersecting points of the limit cycle with the planes U_1 and U_{-1} by a, b, c, and d. The trajectory enters the D_0 region via points b and d and leaves the D_0 region via points a and c. The positions of the points a and c are symmetrical. So are the points b and d. As the value of C_2 increases, the limit cycle deforms continuously but is still symmetric. At some critical value $C_2 = C_a$, symmetry is broken and the limit cycle becomes asymmetric from then on. For the parameter values given in (1), the value of C_a is somewhere between 0.554 and 0.555. It follows from the symmetry of (3) that when a limit cycle Γ is asymmetric, there must exist another limit cycle that is the odd-symmetric image of Γ. Starting from initial conditions odd-symmetric to the current ones, we can always find it.

For $C_2 > C_a$, the positions of points a and c (also, b and d) are no longer symmetric. As c_2 increases, all of them will move towards the right in Fig. 11. This situation persists until some value of C_2 when point d moves exactly on the line $\overline{A^-E^-}$. Since the $E^c(O)$ plane is an eigenspace, the trajectory will remain on it when traveling in the D_0 region. Therefore, the point a is also on the line $\overline{AE}$. However, there is no bifurcation at this value of C_2. If we increase C_2 further, all four points of a, b, c, and d will move to the right of the $E^c(O)$ plane and the limit cycle will also stay all the time to the right of the $E^c(O)$ plane.

When C_2 increases further, at certain value of C_b, the limit cycle becomes unstable and intermittency takes place. By computer simulation, we can only find an approximate value for C_b, which is close to an exact value between 0.558 and 0.559. In Fig. 12(a) we show the Poincare intersection at $x = 1$ (i.e., the U_1 plane) for $C_2 = 0.56$, chosen just a little larger than C_b. (The corresponding trajectory is shown in Fig. 6(c).) In this figure we have also plotted the lines L_0, L_1, L_2 and the points A, B, E. At all points above the line L_2, the trajectory penetrates the U_1 plane from underneath. After it penetrates the U_1 plane, the trajectory will be sucked towards the $E^c(P^+)$ plane very quickly because $|\gamma_1| \gg \sigma_1$. On returning to the U_1 plane, the trajectory almost touches the $E^c(P^+)$ plane and thus always penetrates the U_1 plane downward at points in the wedge area $\angle ABE$ and very close to the line L_1. The Poincare intersection in Fig. 12(a) verifies this. Observe that all downward intersecting points (i.e., points below L_2) are located almost on the line L_1.

Observe next a trajectory starting from point a in Fig. 12(b). It will travel in the D_{+1} region while being attracted towards the $E^c(P^+)$ plane. When it returns to the U_1 plane its intersecting point is b. After leaving b, it will hit the U_{-1} plane at a point symmetric to point c in Fig. 12(b). Then the trajectory enters the D_{-1} region. When it comes back to the U_{-1} plane it will hit a point symmetric to point d in Fig. 12(b). Afterwards the trajectory will travel in the D_0 region and hit back at the U_1 plane. However, in an intermittency situation, the trajectory does not hit the U_1 plane at the same point (point a) this time. Instead, it will hit a point a' which is very close to point a, as depicted in Fig. 12(b). Also, when the trajectory hits back at the U_1 plane from above, the intersecting point will be b', which is very close to point b. The next two intersecting points on the U_{-1} plane will be symmetric to points c' and d', which are very close to points c and d. Thus the trajectory is nearly periodic. In each round, it deviates only a little from the previous round. The map of point a approaches the line L_2 in this manner, i.e., $a \to a' \to \cdots \to a''$, etc. The time waveform in this situation looks nearly periodic and therefore corresponds to the regular phase in Fig. 4(b).

However, when the map of point a gets closer to the line L_2, the situation will change. Remember that $\dot{x} = 0$ for the vector field on the line L_2. When the map of point a is very close to the line L_2, after the trajectory penetrates the U_1 plane from below it will come back rapidly to touch the U_1 plane from above. During this short

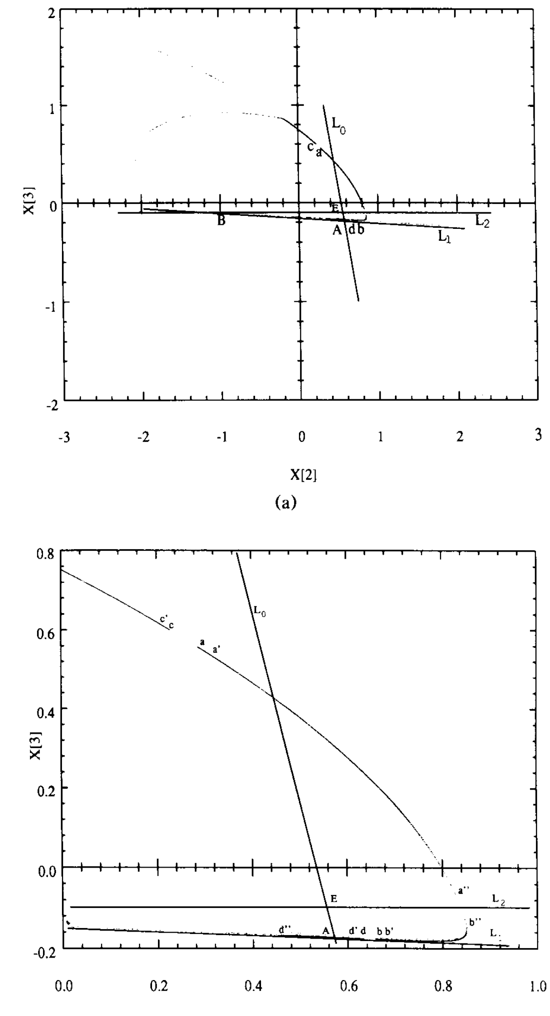

Fig. 12. (a) The Poincare intersection at the $x = 1$ plane for $C_2 = 0.56$. (b) Magnification of Fig. 12(a).

period of time the trajectory has not been compressed close enough to the $E^c(P^+)$ plane. In Fig. 12(b) we can see that the map of point b gradually diverges from the L_1 line. Also, the maps of points c and d in Fig. 12 are moving towards the left. Since they are the asymmetric images of the intersecting points on the U_{-1} plane, the actual intersecting points are moving towards the right. Finally, they will move to such a position that the return trajectory from the U_{-1} plane can no longer reach the U_1 plane. In such a situation, the trajectory will turn back to hit the U_{-1} plane. This type of motion is quite different from the "regular" one and therefore causes a drastic change of the trajectory motion. In Fig. 12(b) observe that the intersecting points near a'' and b'' become more

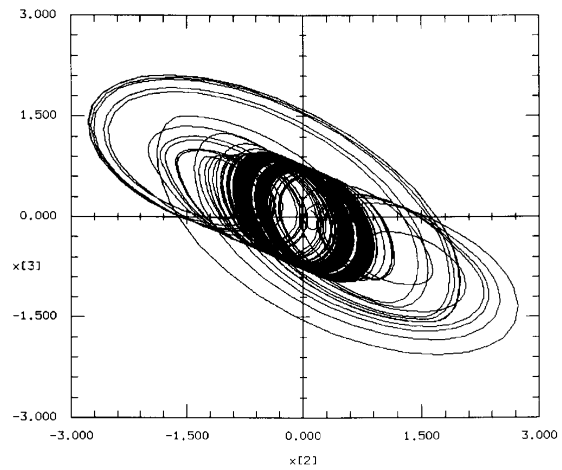

Fig. 13. Trajectories of (v_2, i_3) from computer simulation. $C_2 = 0.56$.

sparse, which means that whenever the trajectory reaches this part, the displacement of each cycle will become bigger. In the one-dimensional map we obtained in Fig. 9 (i.e., the amplitude plot), this situation corresponds to the case where the map moves away from the diagonal. Therefore, the trajectory no longer looks regular and the dynamics change rapidly. The time waveform in this situation therefore corresponds to an irregular burst in Fig. 4(b).

After the trajectory enters an irregular motion regime, it goes wild. However, whenever it penetrates the U_1 or U_{-1} plane, it always goes through $\angle ABE$ and $\angle A^-B^-E^-$. Once its penetrating point falls into the area representing regular motions (e.g., $0.45 < y < 0.8$ in Fig. 12(b)), everything will repeat again. This is the mechanism of the intermittency in our system.

When traveling in the area of regular motion, the trajectory looks like a band or a ribbon. Due to symmetry, there are two symmetric areas of regular motion in the system. Since the reinjection from "bursts" into "regular motion" is quite "random," the trajectory could equally well inject into either one of the area of regular motion. The complete scenario of the trajectory is therefore composed of two solid "bands" and some sparse "threads" around them. This can also be clearly seen from Fig. 13, the (y, z) projections of the trajectory. We will henceforth refer to this trajectory as a "double band attractor."

V. Concluding Remarks

1) We have presented an example of intermittency in the Chua's circuit family. This result enriches the dynamics and shows that all three major routes to chaos can be found in this circuit family.

2) The intermittency phenomenon from the circuit in Fig. 1(a) is a co-dimension 1 bifurcation. Hence, if we adjust any other parameter instead of C_2, a similar bifurcation course will take place. For example, if we set $R = 0$

in (1), the intermittency will start around $C_2 = 1.05$. In this situation the circuit actually contains one less parameter than the circuit shown in Fig. 1(a). However, in a physical realization the inductor will always contain some resistance. Therefore, the circuit in Fig. 1(a) is more robust and easier to realize in the laboratory.

References

[1] S. Wu, "Chua's circuit family," *Proc. IEEE*, vol. 75, pp. 1022–1032, Aug. 1987.

[2] T. Matsumoto, L. O. Chua, and M. Komuro, "The double scroll," *IEEE Trans. Circuits Syst.*, vol. CAS-32, pp. 797–818, Aug. 1985.

[3] L. O. Chua, M. Komuro, and T. Matsumoto, "The double scroll family," *IEEE Trans. Circuits Syst.*, vol. CAS-33, pp. 1073–1118, Nov. 1986.

[4] T. Matsumoto, L. O. Chua, and M. Tokunaga, "Chaos via torus breakdown," *IEEE Trans. Circuits Syst.*, vol. 34, pp. 240–253, Mar. 1987.

[5] T. S. Parker and L. O. Chua, "The dual double scroll equation," *IEEE Trans. Circuits Syst.*, vol. 34, pp. 1059–1073, Sept. 1987.

[6] C. P. Silva and L. O. Chua, "The overdamped double-scroll family," *Int. J. Circuit Theory and Appl.*, vol. 16, pp. 233–302, 1988.

[7] P. Bartissol and L. O. Chua, "The double hook," *IEEE Trans. Circuits Syst.*, vol. 35, pp. 1512–1522, Dec. 1988.

[8] L. O. Chua and G. N. Lin, "Canonical realization of Chua's circuit family," *IEEE Trans. Circuits Syst.*, vol. 37, pp. 885–902, July 1990.

[9] T. S. Parker and L. O. Chua, "INSITE—A software toolkit for the analysis of nonlinear dynamical systems," *Proc. IEEE*, vol. 75, pp. 1081–1089, Aug. 1987.

[10] ——, *Practical Numerical Algorithms for Chaotic Systems.* New York: Springer-Verlag, 1989.

[11] H. G. Schuster, *Deterministic Chaos.* Berlin: Physik-Verlag GmbH, 1984.

Leon O. Chua (S'60–M'62–SM'70–F'74), for a photograph and biography, please see page 243 of the March 1991 issue of this TRANSACTIONS.

Guin-nian Lin received the diploma in electrical engineering from the Shanghai Jiaotong University, Shanghai, China in 1962 and the diploma in circuit theory from the Graduate Division of the same university in 1966.

From 1966 to 1973 he was with the Shanghai Jiao-tong University. In 1973 he joined the Department of Electrical Engineering at the Shanghai Railroad Institute, where he is currently an Associate Professor. During 1980–1982 and 1988–1991, he was with the Electronics Research Laboratory, University of California, Berkeley, as a visiting scholar. His research interest include general circuit theory and nonlinear dynamics.